Lithium-Ion battery SOC estimation

by

Sepideh Afshar

Thesis submitted to the
Faculty of Applied Mathematics
In partial fulfillment of the requirements
For the Ph.D. degree in
Applied Mathematics

School of Applied Mathematics
Faculty of Mathematics
University of Waterloo

Abstract

In recent years, electric and hybrid vehicles (EV/EHV) are becoming more attractive because of higher fuel efficiency and lower emissions. Batteries are the storage unit of electric vehicles and cells are their elementary units. Tracking the state-of-charge (SOC) of each cell in a battery pack is a key requirement for calculating the vehicle's range and driver's peace of mind. Although direct and precise measurement of SOC of a cell is not achievable by existing sensors, other quantities like battery terminal voltage and current can be easily measured. At every measurement step, the cells SOC is determined and updated via the available measurements.

The importance of accurate estimation of SOC is even more crucial in HEVs comparing to EVs since their environment characteristics are more demanding. Therefore, an appropriate method of more accurate estimation of SOC from available measurements are needed. In general, electrochemical model-based estimation methods provide higher accuracy; however, simplifying the governing equations is required to their complexity. So far, the simplified models in the literature lack the accuracy in estimatining SOC for chemical compositions like Lithium ion phosphate, LiFePO4, (LFP) at high current rates. The main weakness of these models is the poor approximation of cell's hysteretic behavior, a critical phenomenon in LFP cell's response.

As the first step of designing an observer, the electrochemical model must be studied for its important features including the nonlinearities, the properties of equilibrium points, and observability. The simplified model must preserve the affecting portion of the dynamics, the location and properties of the equilibrium points and the observability of the state vector. In this report, the electrochemical governing equations are first simulated in COMSOL to investigate the existence of hysteresis in system response. After finding the equilibrium solutions of the system, a simplified model based on linearizing the system around some equilibrium points is developed. Next, sliding mode observer is introduced as a robust observer for SOC estimation.

Contents

List of Tables

List of Figures

Chapter 1

Introduction

In recent years, electric and hybrid vehicles (EV/EHV) are becoming more attractive because of higher fuel efficiency and lower emissions. Batteries as the storage unit of electric vehicles plays an important role. Accurate estimation of the battery's state of the charge is crucial for calculating the vehicle's range and driver's peace of mind. In this chapter, the problem of estimating the battery state is introduced, and different studies on this topic are reviewed.

1.1 Battery management system and state of charge

Among different chemical composition, lithium-ion chemistry is one of the most promising option for the batteries used for EV/HEVs. Delivering high power and energy density, lack of memory effect, low self discharge and high life cycle are referred as the main characteristics of lithium-ion chemistry in comparison to other cell chemistries [22, 42, 25]. Frequent recharging the nickel-cadmium and nickel-metal-hydride batteries after they are partially discharged leads to loss of usable capacity. This phenomenon is called memory effect. Lithium ion phosphate, LiFePO4, (LFP) offers the advantage of better lithium insertion over other alternatives. Its numerous features has drawn considerable interest. Some of these features are listed in [53].

Cells are elementary units of a battery pack. One or more battery packs having different cell configurations may be utilized in EV/HEVs. Therefore, an adequate management system is required to monitor, diagnose and synchronize among the battery cells. This unit is called battery management system (BMS) [25]. Safety and aging are the important issues which must be overcome by a BMS. For this reason, BMS is required to

monitor the state of the battery and perform organized charging and discharging strategy of the cells [22].

Tracking the state-of-charge (SOC) of each cell in a battery pack is a key role of a BMS. At every measurement step, the cells SOC estimation is updated via measuring the terminal voltage, current and temperatures. In practice, SOC can be defined as an indication of the amount of remaining charge inside the cell. A number between 0% to 100% is assigned to this indication. Precise estimation of SOC is important since [35]:

- In contrast to gasoline tank, the batteries can be overcharged or undercharged without accurate SOC estimation.
- It lets the driver use the entire battery capacity.
- The battery pack can be used more effectively when an accurate SOC is available; thus, lighter battery packs could be used.
- The maximum available charge is given by SOC estimation. In this case, less cycles of charging is required and the life cycle is improved.
- SOCs of the cells in a battery pack are utilized by the BMS to balance the state of cells. They become out of balance by time due to the small differences in their dynamics. It may happen when one cell is at high SOC limit while some other cells are in low SOC limit. In a drive cycle of HEVs, balancing of the cells state is done by boosting the cells with low SOC and bucking the cells with high SOC [35].

The importance of accurate estimation of SOC is even more crucial in HEVs comparing to EVs since their environment characteristics are more demanding. While the absolute value of the current rates peaks in EVs are not more than 5C, HEVs draws current rates up to 20c. Moreover, the profile of the current rate shows more dynamics in HEVs since their are designed to overcome the sudden load transitions via battery/motor couple [35, 33]. This means that an efficient estimation method is required to accurately calculate SOC from available measurements.

Although direct and precise measurement of SOC of a cell is not achievable by existing sensors, other quantities like battery terminal voltage and current can be easily measured. The importance of accurate SOC evaluation necessitates a more acceptable method of estimation from available measurements. Different estimation methods proposed in the literature are categorized as direct measurements, indirect/book-keeping and model based/adaptive methods [41].

1.2 Overview of present work on SOC estimation

An inaccurate but cheap method of SOC estimation is online measurement of current and/or terminal voltage resulting in an approximate value of the SOC. Examples can be found in [42, 44, 18]. This method highly depends on temperature, charge/discharge rate and aging [41]. Open circuit voltage (OCV) measurement can be offered as an alternative measurement whose assignment to SOC depends on less factors. In this case, a long resting time must be passed before measuring the value of OCV. Once OCV is achieved at a steady condition, the SOC can be calculated as the inverse image of SOC-OCV map. OCV measurement is not proper for real-time application and highly depends on environmental conditions especially the flowing current rate and hysteresis effect [36].

Impedance measurement is a method of SOC estimation. It is defined as the transfer function from current to voltage signal. The impedance carries information about linear dynamics of the cell. The required data for identifying the impedance is gathered through a test called electrochemical impedance spectroscopy (EIS) test. The parameters of the identified transfer function can be used to estimate the SOC [46]. A good review on SOC estimation by EIS can be found in [43]. Not being applicable in real time application, not including the cell nonlinear behavior, and being sensitive to environmental temperature are some of limitations of impedance technique in SOC estimation [36, 17, 34].

The second category of SOC estimation method relies on measuring and integrating the current. This technique is called coulomb counting. Coulomb counting compensated for battery effects like discharge efficiency, self discharge, and capacity loss is called book-keeping method [41]. Application of coulomb counting in SOC estimation can be found in [3, 60, 40, 5, 36, 1, 39, 23, 4, 24]. Some important factors reducing the estimation accuracy of coulomb counting are temperature, charge and discharge efficiencies, and cycle life [41]. More importantly, the cumulative effect introduced by integration approximation makes the estimation sensitive to measurement errors due to noise, resolution and rounding [3].

Both direct and book-keeping methods experience imperfection when it comes to the dynamics of cell behavior. In order to provide real-time utilization, the estimation method should include the dynamics of cell and variation of SOC. Model based estimation is suggested as a more reliable way of keeping the SOC prediction updated in HEVs. In the literature, this estimation method is also called adaptive SOC estimation system [41]. It uses the information from direct or book-keeping systems and a model representing the cell dynamics to evaluate the SOC. Therefore, an important element of the model

based estimation is the mathematical representation of the cell response.

For the purpose of model-based SOC estimation and BMS improvement, among different models, equivalent circuit models are mostly reported in the literature. Simplicity and relatively few number of parameters are the main characteristics of these models [15]. An equivalent circuit model is composed of basic elements, resistors, capacitors, and voltage source, in the form of a circuit network. Normally, the circuit includes a large capacitor or a voltage source to represent the OCV effect, and the rest of the circuit defines the cell's internal resistance and the cell's dynamics [14].

Hysteresis is a part of cell behavior and exhibits the dependency of the response to the charging/discharging history. Five groups of equivalent circuit models are introduced and tested in [36] in three of which the hysteresis effect is added. Next, an observer compatible with the selected model and the rate of variations must be chosen to predict SOC. Stochastic open-loop estimation is the simplest model-based method which used in [33] to estimate OCV; this estimation value is then mapped to SOC using a linear function. Kalman filtering (KF) is the most cited technique in which compensating for measurement noise is the main property.

One of the first and important efforts on SOC estimation by KF is the comparative studies introduced in [37] and applied in [27]. Because of the model's nonlinearity, extended Kalman filtering (EKF) is applied wherein the model is linearized around the most recent updated estimate. They have also provide their estimation method with the possibility of real-time parameter adaptation by an approach called dual EKF. The major drawback of this method is that there is no proof of convergence of parameters estimation including SOC to the exact values. Similar application of KF or EKF to the equivalent circuit model for SOC estimation can be found in [3, 57, 7, 14].

Dealing with the model nonlinearity can be evaluated by using sigma-point Kalman filtering (SPKF). Utilizing SPKF in observing SOC from voltage measurement is improved in [38, 49]. In this work, the modeling parameters are also let to have small variation in time. Next, two variations of an adaptive approach are improved to update the parameters with no proof of convergence. It should be mentioned that KF is strongly sensitive to model accuracy. Some other examples of equivalent circuit model-based estimation methods are briefly listed here. Sliding mode observer is offered in [19, 20, 32]. Adaptive observer is suggested based on linear model in [59] and nonlinear model in [45]. Luenberger observer which is an error rejection observation method is used for a nonlinear model in [26] and for a linear parameter varying model in [16, 25].

Equivalent circuit models are not advised in real-time HEV application for SOC

estimation. They suffers from poor modeling at high transient loads, rough modeling of hysteresis, and dependency of modeling parameters on SOC. In this cases, more accurate and physical models are required. Electrochemical models are preferred to equivalent circuit models since they closely represent the physical behavior inside the cell. Therefore adding the effect of temperature and modeling the aging phenomenon, the inherent features of Li-ion batteries, are more feasible. Unfortunately, the electrochemical models are not applicable for real-time observation because of their complexity.

A review on most simplified electrochemical models is given in [47]. Single particle model (SPM) is a common way of handling the unwanted complexities. This model is made by the assumptions that the electrodes are made of a single spherical particle, there is no change in concentration and potential of the electrolyte, and the parameters are constant. It is coupled with averaging the concentration of active material in [48] to construct ODE representation and estimate SOC by EKF. Averaging over the entire electrode region is also used in [6, 21, 22] wherien observation is evaluated by respectively EKF and output injection-based observer combined with mass conservation law.

Taking Laplace transform with respect to time is used in [51, 52] to find the impedance transfer function. Then, a set of ODEs is constructed by taking Laplace inverse transform. Afterwards, KF is used to estimate the SOC. More accurate observation method is given in [29, 31, 30]. In this case, transforming the system to ODEs via Laplace transform is used as a way of identifying the system parameters using impedance technique. An output injection observer is applied in both system dynamics and boundary conditions in a SPM, and Backstepping approach is employed to design the gains.

In general, electrochemical model-based estimation provide higher accuracy; however, simplifying the governing equations is required to to their complexity. So far employed simplified models loose their utility for chemical compositions like LFP at high current rates and dynamics. More accurate approximation of original equation which is simple enough to be solved in real-time SOC estimation is required. Typically, a state estimator is composed of a copy of model and a feedback from output measurement. When being complemented by simplification assumption, an efficient observer must provide enough accuracy and robustness to modeling uncertainties.

The goal of this project is to predict the battery SOC during a drive cycle; thus, a simplified model and a robust observer need to be designed. Electrochemical model is considered to represent every cell behavior. As the first step, the electrochemical model must be studied for its important features including the nonlinearities, the properties of equilibrium points, and observability. A simplified model must next be developed. This

simplified model must preserve the affecting portion of the dynamics, the location and properties of the equilibrium points and the observability of the state vector. Linear approximation of the PDAEs augmented with sliding mode observer will be used as explained later in this report.

The main objectives of this research can be summarized as follow:

- In most of the works done on modeling and simulation of Li-ion batteries, OCV is assumed to be a single value function. Investigating the validity of this assumption is critical especially for LFP cells. Next, the OCV hysteretic profile must be modeled if its importance is approved.

- After finding the equilibrium points of the system, a simplified model is developed based on linearizing the system around some equilibrium points.

- The developed linearized system is then approximated by a set of ODEs without limiting the order of system. Afterwards, an order reduction method is used to construct a system of ODEs applicable in real time environment.

- A robust observer is designed to consider the system uncertainties. At this step, the bound on system nonlinear part and uncertainties is found. Given the bound, the dropped dynamics of the system is compensated by proper gain design. Sliding mode observer is suggested to achieve this end.

- Finally, the observer design is extended to include the variation of modeling parameters due to the effect of aging and temperature.

This document is organized as follows. In Chapter 2, the battery modeling from electrochemical point of view is discussed. In this chapter, the electrochemical governing equations which are a set of PDAEs are evaluated for LPF cell. Furthermore, the hysteresis effect generated by the system dynamics is studied. The system is then written in the form of state space representation. The evaluated equations are used in Chapter 3 to initiate the linear approximation of the system. Finally, the future works are described in Chapter 4 where the potential observation method, sliding mode observer, is introduced.

Chapter 2

Mathematical modeling

In this research, Li-ion cells whose positive electrode is made of LFP material are chosen as the chemistry of interest. Most of the theories in electrochemical modeling are developed for battery chemistries like lead acid and nickel-metal hydride. The mathematical modeling of Li-ion cells was first developed by Doyle et al. [8]. Their recent formulation presented in [56] constructs the majority of the equations used here.

2.1 Electrochemical model

A battery is composed of three major parts, the positive electrode, negative electrode and separator. In a Li-ion cell, the negative electrode (n) is made of carbon and the positive electrode (p) is a metal oxide. Two electrodes are separated by a separator and all three regions are immersed in an electrolyte. The cell is sketched in Figure 2.1. In practice, the electrodes are composed of a slurry of active material, conductive filler, and binder coated onto a foil current collector. Therefore, a porous structure is provided. In order to derive the governing equations two important theorems are solicited: porous electrode theory and concentration solution theory.

In porous electrode theory, considering the exact position and shape of the pores and particles in the electrode porous structure is substituted by utilizing average properties over a control volume, small compared to the electrode width and large compared to pores size. Accordingly, the electrodes are treated as the superposition of the active material particles, filler, and electrolyte coexisting at the same point. In concentration theory, the interaction of solution species' with solvent as well as their mutual interactions are studied. The electrolyte in Li-ion cells is usually composed of a single salt in a homo-

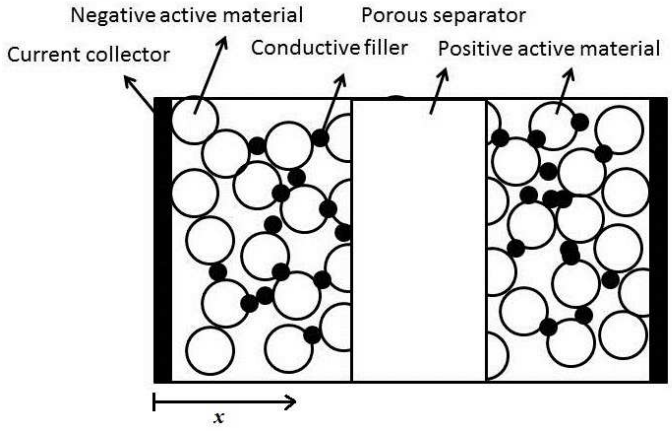

Figure 2.1: a Li-ion battery cell

geneous solvent, and its behavior is addressed in [54] to accord with the concentrated solution theory.

Given spherical shape to the active material particles, the following parameters can be defined from superposition assumption of the electrode and electrolyte phase. The interfacial area between two phases per unit volume and the volume fraction of each phase are respectively defined by $a = 3\epsilon_s/R$ and $\epsilon = N_P 4\pi R^3/3$ where R is the radius of spherical particles, ϵ_s is the volume fraction of the electrode phase, and N_P is the number of particles per unit volume.

The volume fraction coefficient of each phase is then used to modify the cell properties affected by porosity. Bruggeman relation is used to address porosity effect. Therefore, effective solid-phase conductivity, electrolyte diffusivity, and electrolyte conductivity are respectively defined by $\sigma^{eff} = \sigma\epsilon_s^P$, $\kappa^{eff} = \kappa\epsilon_e^P$, and $D_e^{eff} = D_e\epsilon_e^P$ where P is the Bruggeman exponent. This value is usually set to 1.5 for Li-ion cells.

In this research, the representative variables are assumed to change only along the cell. Therefore, 1D electrochemical modeling of cell is considered in this chapter. Four variables are used to represent the cell behavior. These variables are concentration of lithium in solid phase $c_s(r, x, t)$ and lithium ions in electrolyte phase $c_e(r, x, t)$ as well as electric potential of solid phase $\varphi_s(x, t)$ and electrolyte phase $\varphi_e(x, t)$.

A Li-ion cell works based on the principle of lithium insertion/deinsertion where electrons are consumed or produced. In LFP electrodes, this mechanism is a two phase process taking place between the lithium poor phase, $Li_\epsilon FePO_4$, and the lithium rich phase, $LI_{1-\epsilon}FePO_4$. The two-phase behavior plays an important role in the cell response

and must be considered in the modeling process. A few models are improved in the literature to conduct the two-phase behavior in LFP cells. Among them, variable solid-state diffusivity (VSSD) model is used here because of being the trade off between simplicity and physical accuracy. The details on VSSD model can be found in [55, 12, 11].

The time variation of lithium concentration can be found by conservation law of lithium ions in every particle. Solving for more than one particle at every position in the electrode elevates the modeling accuracy. Further asumptions are negligible volume change and high conductivity of solid phase in the process of lithium insertion/deinsertion. The solid-phase mass balance of lithium in a single particle is then described by the second Fick's law in the form of diffusion equation as

$$\frac{\partial c_{s,k}(x, r_k, t)}{\partial t} = \frac{1}{r_k^2}\frac{\partial}{\partial r_k}(D_{s,k}\frac{1}{r_k^2}\frac{\partial}{\partial r_k}c_{s,k}(x, r_k, t)) \tag{2.1}$$

where the sub-index $k = 1 \cdots K$ corresponds to the index of particle size bins and $D_{s,k}$ is the diffusion coefficient of kth size bin. The diffusion coefficient is a function of lithium concentration and is defined by

$$D_{s,k} = \alpha_k \mathcal{D}_s \tag{2.2}$$

where $\mathcal{D}_s$ is solid state binary diffusion coefficient and

$$\alpha_k = -\frac{F}{RT} y_k(1 - y_k)\frac{\partial U_k(y_k)}{\partial y_k}, \quad y_k = \frac{c_{s,k} \mid_{r_k = R_k}}{c_{s,max}}.$$

In this expression, U_k is the open circuit potential (OCP) for kth size bin and $c_{s,max}$ is the maximum solid state concentration. OCP is defined for every size bin of each electrode as a function of the solid concentration on the particle surface $c_{s,k} \mid_{r_k = R_k}$ and with respect to a hypothetical lithium reference electrode.

Finally, the diffusion equation is completed via the boundary conditions given by

$$\frac{\partial c_{s,k}}{\partial r_k} \mid_{r_k = 0} = 0, \quad D_{s,k}\frac{\partial c_{s,k}}{\partial r_k} \mid_{r_k = R_k} = \frac{i_k}{F}$$

where R_k is the radius of, i_k is the reaction current at the surface of kth size bin and F is Faraday's constant. The total number of K diffusion equations of the form 4.4 must be solved in both electrode regions but not in separator.

Next phenomenon to be modeled is lithium ion concentration in the electrolyte phase. Lithium ions are the positive ions of a typical Li-ion cell. In charging process, they are produced at positive electrode solid/electrolyte interface, travel through the electrolyte, and are consumed at negative electrode. Therefore, the concentration distribution of

these ions over the cell plays an important role in the electrochemical reactions. The main assumptions in this step are ignoring convection in the electrolyte, side reaction in electrolyte, volume change of solid phase due to lithium insertion/deinsertion process and having binary electrolyte (a binary electrolyte includes only two groups of ions). The lithium ion concentration in the electrolyte is defined by

$$\epsilon_e \frac{\partial c_e(x,t)}{\partial t} = \frac{\partial}{\partial x}(D_e^{eff} \frac{\partial c_e(x,t)}{\partial x}) + \frac{1-t_+^0}{F} \sum a_k i_k \tag{2.3}$$

where D_e^{eff} is the electrolyte effective diffusion coefficient and t_+^0 is the transference number of lithium ion with respect to the solvent velocity.

Since there exists electrolyte in every spot of the cell, equation 2.3 must be solved in all three regions, negative electrode, positive electrode and separator. The boundary conditions are defined by zero flux at the current collectors as

$$\frac{\partial c_e}{\partial x} \mid_{x=0} = \frac{\partial c_e}{\partial x} \mid_{x=L} = 0$$

where L is the length of cell. A more general form of equation 2.4 can be found in [54].

The potential in the electrolyte is established for binary electrolyte which is a typical choice for most of the Li-ion battery. When employing the lithium metal as the reference electrode and 1:1 binary electrolyte, this gradient is defined by [54]

$$\frac{\varphi_e(x,t)}{\partial x} = \frac{-i_e}{k^{eff}} + \frac{2RT(1-t_+^0)}{F}(1 + \frac{d \ln f_\pm}{d \ln c_e}) \frac{\partial \ln c_e(x,t)}{\partial x} \tag{2.4}$$

where R is the gas constant, i_e is the current assigned to the electrolyte phase, and $f_\pm$ is the mean molar activity coefficient in the electrolyte.

By using the electroneutrality of the electrolyte phase, a current balance gives the relation between the current divergence and the net pore-wall reaction flux as

$$\frac{\partial i_e(x,t)}{\partial x} = \sum a_k i_k. \tag{2.5}$$

Now, by substituting equation 2.5 into 2.4 the potential satisfies the expression

$$\frac{\partial}{\partial x}(k^{eff} \frac{\partial \varphi_e(x,t)}{\partial x} + k_D^{eff} \frac{\partial \ln c_e(x,t)}{\partial x}) = \sum a_k i_k \tag{2.6}$$

where $k_D^{eff} = k^{eff} \frac{2RT(1-t_+^0)}{F}(1 + \frac{d \ln f_\pm}{d \ln c_e})$. The boundary conditions are defined by

$$\frac{\partial \varphi_e}{\partial x} \mid_{x=0} = \frac{\partial \varphi_e}{\partial x} \mid_{x=L} = 0$$

These boundary conditions do not completely define the problem, and extra conditions are required which is defined in the next section.

Finally, the potential in the solid phase of the porous electrode is derived from Ohms Law as

$$\sigma^{eff}\frac{\varphi_s(x,t)}{\partial x} = i_e(x,t) - I(t) \tag{2.7}$$

where $I(t)$ is the current, and $i_s(x,t) = I(t) - i_e(x,t)$ is the current in the solid phase. By substituting equation 2.5 into 2.7, the solid potential must satisfy

$$\frac{\partial}{\partial x}(\sigma^{eff}\frac{\varphi_s(x,t)}{\partial x}) = \sum a_k i_k \tag{2.8}$$

The boundary conditions are given by the fact that the electrolyte current density is zero at current collectors/electrodes interface and equals the total current, $I(t)$ at electrodes/separator interface. Moreover, the solid potential is set zero at one of the current collectors as the reference value. In general, the boundary conditions are

$$\varphi_s \mid_{x=0} = 0, \quad \frac{\partial\varphi_s}{\partial x} \mid_{x=\delta_n} = \frac{\partial\varphi_s}{\partial x} \mid_{x=\delta_n+\delta_{sp}} = 0, \quad \sigma^{eff}\frac{\partial\varphi_s}{\partial x} \mid_{x=L} = I(t)$$

where δ_n is the length of negative electrode, and δ_{sp} is the length of the separator.

Solving the electrochemical governing equations with the defined boundary conditions gives the potential in the solid phase such that the total amount of reaction along the electrode equals to the applied current [54]. The output of the system is set as the terminal voltage. By including the effect of external load, terminal voltage has the form of

$$V(t) = \varphi_s(L,t) - \varphi_s(0,t) - R_l I(t) \tag{2.9}$$

where R_l is the load resistance.

In the evaluated mathematical equations, local electrochemical reaction rate, i_k, is an essential term. It can be determined as a function of concentration and potential. Butler-Volmer rate equation is usually used for this purpose, and for every size bin, is defined by

$$i_k = i_{0,k}\{\exp(\frac{\alpha_a F\eta_k}{RT}) - \exp(-\frac{\alpha_c F\eta_k}{RT})\} \tag{2.10}$$

where $i_{0,k}$ is the exchange current density, α_a and α_c are anodic and cathodic transfer coefficient, and

$$\eta_k = \varphi_s - \varphi_e - U_k(y_k) \tag{2.11}$$

is the overpotential term. The exchange current density is defined by

$$i_{0,k} = \kappa(c_e)^{\alpha_a}(c_{s,max} - c_{s,k} \mid_{r_k=R_k})^{\alpha_c}(c_{s,k} \mid_{r_k=R_k})^{\alpha_a} \tag{2.12}$$

where κ is a kinetic rate constant.

The second and more important term in the electrochemical model is the OCP term, U_k. The OCP profile has an important effect on simulation result and must be identified carefully. This effect is even more critical when comparing the simulation results for a full cell sandwich with experimental data. Therefore, accurate data on measurement of this quantity with respect to a lithium reference electrode must be collected. Moreover, an adequate physical or empirical model must be chosen to determine the shape of OCP profile. The OCP term is given in a look-up table for numerical simulation and can be approximate by

$$U_k : \mathbb{R}^+ \to \mathbb{R} \tag{2.13}$$

$$y_k \mapsto h_k(y_k) \tag{2.14}$$

where $y_k = (c_{s,k} \mid_{r_k=R_k})/c_{s,max}$ and $f_k \in C^\infty(\mathbb{R}^+)$. It should be noted that f_k is defined for every electrode.

In the experiment level of OCP identification, both solid concentration at particle surface and the half cell open circuit voltage must be measured. Open circuit voltage can be easily measured after a long rest time since the current is turned off; however, measuring the solid concentration is not directly achievable. Given the assumption that the solid concentration reaches a uniform distribution after a long rest time, it is suggested to be determined by coulomb counting method. The number of electrons which leaves or enters into the electrode divided by the solid phase volume specifies the change in the solid concentration.

For collecting the required data, the half cell is discharged (charged) from fully charged (discharged) state in successive charging (discharging) periods. In every period, the cell is charged (discharged) by a fixed value with a constant current rate; thus, error augmentation would not be an issue in integral calculation of current. Experimental results display different values for OCP in charging and discharging cycles at a specific SOC. In other words, the variation of OCP with respect to solid surface concentration is hysteric. Furthermore, this hysteresis is also observed to be rate dependent.

2.2 Hysteresis

The same hysteretic behavior as OCP is observed in a full cell terminal voltage measurements. From the definition of overpotential, equation 2.11, the output equation 2.9 is

transformed to

$$V(t) = U_k(y_k \mid_{x=L}) - U_k(y_k \mid_{x=0}) + \eta_k(L,t) - \eta_k(0,t) + \varphi_e(L,t) - \varphi_e(0,t). \qquad (2.15)$$

It shows that the terminal is the superposition of OCP change and the change in the space variables, overpotential and electrolyte potential. Therefore, even if the OCP is a single value function, there is still possibility of hysteretic behavior arising from the system dynamics. A definition for hysteresis is required to investigate the role of system states in terminal voltage hysteresis.

Definition 2.1. [28]
A system is said to include hysteresis if there exists persistent non-trivial closed curve in its input-output mapping when it is existed by periodic inputs with frequencies going to zero.

Proving the existence of the persistent closed loop is not achievable in many cases. However, simulation results indicate whether the system response shows hysteresis. The cell dynamic equations can be tested via definition 2.1 with several sinusoidal current inputs with different frequencies. COMSOL software is used here to solve the governing equations, 2.1, 2.3, 2.6, and 2.8, via finite element method (FEM). The results are shown in Figures 2.2, 2.3, and 2.4. The simulation is set for constant solid diffusion coefficient and one particle size bin. From simulation results, it can be seen that a closed loop is initiated when the input frequency gets smaller. This closed loop is persistent for small frequency values; however, the simulation long run time limits testing smaller frequencies than $0.001s^{-1}$.

2.3 State space representation

Set the number of particle size bins to $K = 2$, and the transfer coefficient to $\alpha_a = \alpha_c = 1/2$. Let

$$\begin{aligned}
&\mathcal{X} = \mathcal{L}^2(0,L) \times \mathcal{L}^2([0,L_1] \times [0,R_1]) \times \mathcal{L}^2([0,L_1] \times \\
&[0,R_2]) \times \mathcal{L}^2([L_2,L] \times [0,R_1]) \times \mathcal{L}^2([L_2,L] \times [0,R_2]) \\
&\mathcal{Y} = \mathcal{L}^2(0,L) \times \mathcal{L}^2(0,L_1) \times \mathcal{L}^2(L_2,L) \\
&\mathcal{C} = \mathcal{H}^2(0,L) \times \mathcal{H}^2([0,L_1] \times [0,R_1]) \times \mathcal{H}^2([0,L_1] \times \\
&[0,R_2]) \times \mathcal{H}^2([L_2,L] \times [0,R_1]) \times \mathcal{H}^2([L_2,L] \times [0,R_2]) \\
&\mathcal{P} = \mathcal{H}^2(0,L) \times \mathcal{H}^2(0,L_1) \times \mathcal{H}^2(L-2,L)
\end{aligned}$$

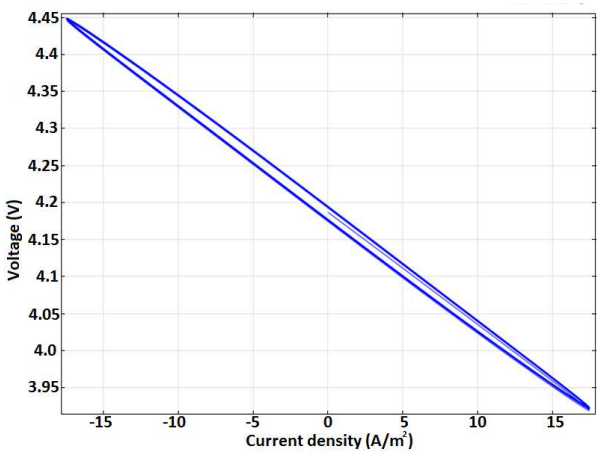

Figure 2.2: Current-voltage mapping for $I(t) = (1)\sin(t)$

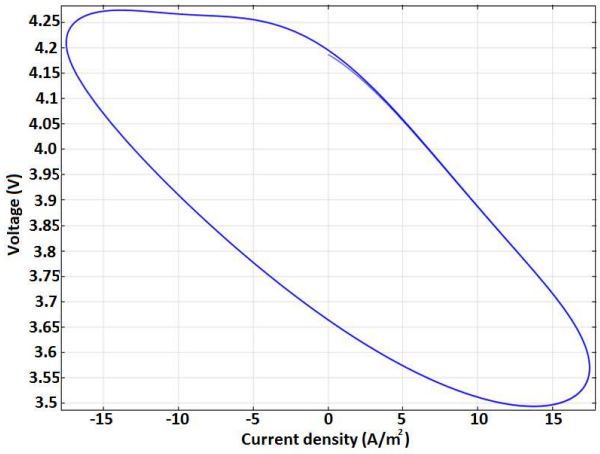

Figure 2.3: Current-voltage mapping for $I(t) = (1)\sin(0.001t)$

where $L_1 = \delta_n,\ L_2 = \delta_n + \delta_{sp}$ Let $\boldsymbol{c} = [c_1, c_{2,n}, c_{3,n}, c_{2,p}, c_{3,p}]^T = [c_e, c_{s,1}\ |_{[0,L_1]}, c_{s,2}\ |_{[0,L_1]}, c_{s,1}\ |_{[L_1,L_2]}, c_{s,2}\ |_{[L_1,L_2]}]^T \subseteq \mathcal{X}$ be the state vector and $\boldsymbol{\varphi} = [\varphi_1, \varphi_{2,n}, \varphi_{2,p}]^T = [\varphi_e, \varphi_s\ |_{[0,L_1]}, \varphi_s\ |_{[L_1,L_2]}]^T \subseteq \mathcal{Y}$. Then, the state space representation of cell governing equations are written in the form of

$$\begin{bmatrix} \dot{\boldsymbol{c}} \\ 0 \end{bmatrix} = A \begin{bmatrix} \boldsymbol{c} \\ \boldsymbol{\varphi} \end{bmatrix} = \begin{bmatrix} A_1 \\ A_2 \end{bmatrix} \begin{bmatrix} \boldsymbol{c} \\ \boldsymbol{\varphi} \end{bmatrix} \tag{2.16}$$

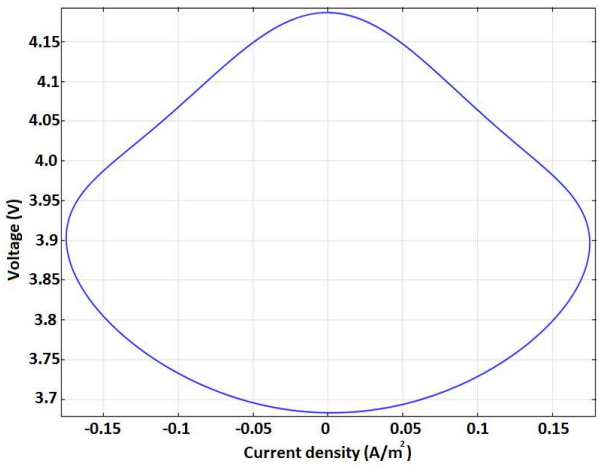

Figure 2.4: Current-voltage mapping for $I(t) = (0.01)\sin(0.00001t)$

where, $A_1 : \mathcal{C} \times \mathcal{P} \to \mathcal{X}$, $A_2 : \mathcal{C} \times \mathcal{P} \to \mathcal{X}$ have the form

$$A_1 \begin{bmatrix} \boldsymbol{c} \\ \boldsymbol{\varphi} \end{bmatrix} = \begin{bmatrix} \frac{\partial}{\partial x}(D_e^{eff}\frac{\partial}{\partial x}(c_1)) + \frac{1-t_+^0}{F}\sum a_k i_k(\boldsymbol{c},\boldsymbol{\varphi}) \\ \frac{1}{r_1^2}\frac{\partial}{\partial r_1}(D_{s,1}\frac{1}{r_1^2}\frac{\partial}{\partial r_1}(c_{2,n})) \\ \frac{1}{r_2^2}\frac{\partial}{\partial r_2}(D_{s,2}\frac{1}{r_2^2}\frac{\partial}{\partial r_2}(c_{3,n})) \\ \frac{1}{r_1^2}\frac{\partial}{\partial r_1}(D_{s,1}\frac{1}{r_1^2}\frac{\partial}{\partial r_1}(c_{2,p})) \\ \frac{1}{r_2^2}\frac{\partial}{\partial r_2}(D_{s,2}\frac{1}{r_2^2}\frac{\partial}{\partial r_2}(c_{3,p})) \end{bmatrix}$$

$$A_2 \begin{bmatrix} \boldsymbol{c} \\ \boldsymbol{\varphi} \end{bmatrix} = \begin{bmatrix} \frac{\partial}{\partial x}(k^{eff}\frac{\partial}{\partial x}(\varphi_1) + k_D^{eff}\frac{\partial}{\partial x}(\ln c_1)) - \sum a_k i_k(\boldsymbol{c},\boldsymbol{\varphi}) \\ \frac{\partial}{\partial x}(\sigma^{eff}\frac{\partial}{\partial x}(\varphi_{2,n})) - \sum a_k i_k(\boldsymbol{c},\boldsymbol{\varphi}) \\ \frac{\partial}{\partial x}(\sigma^{eff}\frac{\partial}{\partial x}(\varphi_{2,p})) - \sum a_k i_k(\boldsymbol{c},\boldsymbol{\varphi}) \end{bmatrix}$$

For $\boldsymbol{c} \in \mathcal{C}$ and $\boldsymbol{\varphi} \in \mathcal{P}$, the boundary conditions are

$$\frac{\partial c_1}{\partial x} \mid_{x=0} = \frac{\partial c_1}{\partial x} \mid_{x=L} = 0 \tag{2.17}$$

$$\frac{\partial c_{k+1,n}}{\partial r_k} \mid_{r_k=0} = 0, \quad k = 1,2 \tag{2.18}$$

$$D_{s,k}\frac{\partial c_{k+1,n}}{\partial r_k} \mid_{r_k=R_k} = \frac{i_k}{F}(\boldsymbol{c},\boldsymbol{\varphi}), \quad k = 1,2 \tag{2.19}$$

$$\frac{\partial c_{k+1,p}}{\partial r_k} \mid_{r_k=0} = 0, \quad k = 1,2 \tag{2.20}$$

$$D_{s,k}\frac{\partial c_{k+1,p}}{\partial r_k} \mid_{r_k=R_k} = \frac{i_k}{F}(\boldsymbol{c},\boldsymbol{\varphi}), \quad k = 1,2 \tag{2.21}$$

$$\frac{\partial \varphi_1}{\partial x} \mid_{x=0} = \frac{\partial \varphi_1}{\partial x} \mid_{x=L} = 0 \tag{2.22}$$

$$\varphi_{2,n} \mid_{x=0} = 0 \tag{2.23}$$

$$\frac{\partial \varphi_{2,n}}{\partial x} \mid_{x=L_1} = 0 \tag{2.24}$$

$$\frac{\partial \varphi_{2,p}}{\partial x} \mid_{x=L_2} = 0 \tag{2.25}$$

where the modeling parameters depends of the properties and structure of the region on which they are defined. Accordingly, they have different values and definition. More details on these parameters and how they are correlated to the region of definition are given in section 2.1

The boundary control is given by

$$-\sigma^{eff} \frac{\partial \varphi_2}{\partial x} \mid_{x=L} = I(t). \tag{2.26}$$

Finally, the electrochemical reaction rate is restated as

$$i_k(\boldsymbol{c}, \boldsymbol{\varphi}) = \begin{cases} \frac{1}{2} i_{0,k}(c_1, c_{2,n}) \sinh^{-1}\left(\frac{F(\varphi_{2,n} - \varphi_1 - U_k(\frac{c_{k+1,n}|_{r_k=R_k}}{c_{s,max}}))}{RT}\right) & \text{if } x \in [0, L_1] \\ 0 & \text{if } x \in [L_1, L_2] \\ \frac{1}{2} i_{0,k}(c_1, c_{2,p}) \sinh^{-1}\left(\frac{F(\varphi_{2,p} - \varphi_1 - U_k(\frac{c_{k+1,p}|_{r_k=R_k}}{c_{s,max}}))}{RT}\right) & \text{if } x \in [0, L_1] \end{cases} \tag{2.27}$$

Chapter 3

Linear approximation

In this chapter, the linear approximation of nonlinear PDAEs is considered for two reasons. First, the stability properties of equilibrium points can be found using the linear approximation around the equlibria under some conditions. In addition, the linearized system is an appropriate choice for model based robust estimation methods. In this case, the linear part of the model is used for the purpose of estimation, and the observer gain is chosen to compensate the uncertainties.

3.1 equilibrium points

In order to find the equilibrium points, differentiation of state variable with respect to time must set zero to find the equilibrium points. The cell model includes a set of PDAEs which must be solved over three connected regions. First, the equilibrium solution is found for negative electrode. let $\partial c_{2,n}/\partial t = 0$ and $\partial c_{3,n}/\partial t = 0$. At negative electrode, from 2.16, $D_{s,2}r_2^2\partial c_{3,s}/\partial x = \zeta_{1,n}$ and $D_{s,1}r_1^2\partial c_{2,n}/\partial x = \xi_{1,n}$ where $\zeta_{1,n}$ and $\xi_{1,n}$ are constants. By using boundary conditions 2.18, $\zeta_{1,n} = 0$ and $\xi_{1,n} = 0$; thus,

$$\frac{\partial c_{k+1,n}}{\partial_{r_k}} = 0 \tag{3.1}$$

for every $(x, r_k) \in (0, L) \times (0, R_k)$ and $k = 1, 2$. Then, equation 3.1 can be substituted in boundary condition 2.19 which leads to

$$0 = -FD_{s,k}\frac{\partial c_{k+1,n}}{\partial_{r_k}} \mid_{r_k=R_k} = i_k \tag{3.2}$$

From 3.1, the equilibrium solid concentration is defined by

$$c_{3,n} = \zeta_{2,n}(x), \quad c_{2,n} = \xi_{2,n}(x) \tag{3.3}$$

where $\zeta_{2,n}$ and $\xi_{2,n}$ are functions of spatial variable x.

Now, let $\partial\epsilon_e c_1/\partial t = 0$. Substituting equation 3.2 into 2.16 results in $D_e^{eff}\partial c_1/\partial x \mid_{x\in[0,L_1]}= \phi_{1,n}$ where $\phi_{1,n}$ is constant. By applying the boundary condition 2.17, it can observe that $\phi_{1,n} = 0$ and $\partial c_1/\partial x = 0 \mid_{x\in[0,L_1]}$; then, the equilibrium electrolyte concentration is obtained as

$$c_1 \mid_{x\in[0,L_1]}= \phi_{2,n} \tag{3.4}$$

where $\phi_{2,n}$ is constant.

Next, the constraint equations, the last two rows of 2.16 defined by the operator A_2, are solved to completely define the equilibrium points. Substituting equation 3.2 into 2.16 gives $\sigma_n^{eff}\partial\varphi_{2,n}/\partial x = \varsigma_{1,n}$ where $\varsigma_{1,n}$ is constant. By using the boundary 2.22, $\varsigma_{1,n} = 0$ and $\partial\varphi_{2,n}/\partial x = 0$. Therefore, the equilibrium solid potential is obtained as

$$\varphi_{2,n} = \varsigma_{2,n} \tag{3.5}$$

where $\varsigma_{2,n} = 0$ by boundary condition 2.23.

In the same way, substituting equation 3.2 into 2.16 gives $k^{eff}\partial\varphi_1/\partial x \mid_{x\in[0,L_1]}= \psi_{1,n}$ where $\psi_{1,n}$ is constant and is defined by the boundary condition 2.24. It follows that $\psi_{1,n} = 0$ and $\partial\varphi_1/\partial x \mid_{x\in[0,L_1]}= 0$. Therefore, the equilibrium electrolyte potential is obtained as

$$\varphi_1 \mid_{x\in[0,L_1]}= \psi_{2,n} \tag{3.6}$$

where $\psi_{2,n}$ is constant.

Moreover, $i_k = 0$ given in equation 2.27 leads to further constraint on equilibrium points. Because $i_{0,k} = 0$ results in trivial solution, the roots of i_k are given by

$$\varphi_{2,n} - \varphi_1 \mid_{x\in[0,L_1]} -U_k(\frac{c_{k+1,n} \mid_{r_k=R_k}}{c_{s,max}}) = 0. \tag{3.7}$$

Therefore, the equilibrium solid concentration takes the form

$$\begin{aligned} c_{2,n} &= c_{2,n} \mid_{r_1=R_1}= \xi_{2,n}(x) = \xi_{3,n} \\ c_{3,n} &= c_{3,n} \mid_{r_2=R_2}= \zeta_{2,n}(x) = \zeta_{3,n} \end{aligned} \tag{3.8}$$

where $\xi_{3,n} = \zeta_{3,n}$ is constant. By the same procedure, the equilibrium solution at separator and positive electrode are constants respectively defined by

$$c_1 \mid x \in [L_1, L_2] = \phi_{2,s}, \quad \varphi_{2,n} = \psi_{2,s} \tag{3.9}$$

and

$$c_1 \mid x \in [L_2, L] = \phi_{2,p}, \quad c_{2,p} = \xi_{3,p}, \quad c_{3,p} = \zeta_{3,p}, \quad \varphi_1 \mid x \in [L_2, L] = \varsigma_{2,p}, \quad \varphi_{2,p} = \psi_{2,p} \tag{3.10}$$

where $\xi_{3,p} = \zeta_{3,p}$. From continuity condition of state variables,

$$\begin{aligned} \phi_{2,n} &= \phi_{2,s} = \phi_{2,p} \\ \psi_{2,n} &= \psi_{2,s} = \psi_{2,p} \end{aligned} \tag{3.11}$$

By employing the condition $\varphi_1 \mid x \in [L_2, L] = \varsigma_{2,p}$ at positive electrode and the boundary condition 2.26, the current $I(t)$ at equilibrium state is determined as

$$0 = -\sigma^{eff} \frac{\partial \varphi_1}{\partial_x} \mid x \in [L_2, L] = I(t) \tag{3.12}$$

In conclusion, there are more than one equilibrium solutions. The history of cell over a period of drive cycle defines the amount of active material left in every electrode. Given the amount of available active material, the equilibrium solution for solid concentration is specified. In addition, the total amount of lithium ions in electrolyte is fixed. Therefore,

$$\phi_{2,j} = c_e^0 \tag{3.13}$$

where j can be n, s, or p and c_e^0 is initial electrolyte concentration.

3.2 Linearization around equilibria

Given the equilibrium points, the variation of the system variables around these points must be investigated in the nest step. Therefore, linearizing the system is studied in this section.

Definition 3.1. [13]
The operator $G : \mathcal{X}_1 \to \mathcal{X}_2$, where $\mathcal{X}_1$ and $\mathcal{X}_2$ are Banach spaces, is said to be Gateaux differentiable at x if there exists a linear operator $dG(x)$ such that

$$\lim_{t \to 0} t^{-1}(G(x + tv) - G(x)) = dG(x)v \quad \forall v \in \mathcal{X}_1.$$

$dG(x)$ is called Gateaux derivative of operator at x.

The state space representation of the cell dynamics is given in equation 2.16. In this equation, the operator A_2 specifies the mapping between the variable vector $\boldsymbol{\varphi}$ and

the state vector $\boldsymbol{c}$. It is solved for $\boldsymbol{\varphi}$ as a function of state vector, and the result is substituted in second equation. First, the system operator is evaluated at the perturbed state vector $\boldsymbol{c} = \boldsymbol{c}^e + t\boldsymbol{c}^h$ where $\boldsymbol{c}^e = [c_1^e, c_{2,n}^e, c_{3,n}^e, c_{2,p}^e, c_{3,p}^e]^T$ is an equilibrium point and $t\boldsymbol{c}^h$ is perturbation term where $\boldsymbol{c}^h = [c_1^h, c_{2,n}^h, c_{3,n}^h, c_{2,p}^h, c_{3,p}^h]^T \in \mathcal{C}$.

The variable vector $\boldsymbol{\varphi}$ can be written as $\boldsymbol{\varphi} = \boldsymbol{\varphi}^e + \boldsymbol{\varphi}^p$, where $\boldsymbol{\varphi}^e = [\varphi_1^e, \varphi_{2,n}^e, \varphi_{2,p}^e]^T$ is equilibrium solution for $\boldsymbol{c}^e$ and $\boldsymbol{\varphi}^p = [\varphi_1^p, \varphi_{2,n}^p, \varphi_{2,p}^p]^T$ is perturbation term. Now, it is proved that for every $\boldsymbol{c} \in \mathcal{C}$ and $\boldsymbol{\varphi} \in \mathcal{P}$ satisfying the equation 2.16 and boundary conditions in equations 2.17-2.25, $\boldsymbol{\varphi}^p = t\boldsymbol{\varphi}^h$ where $\lim_{t\to 0} \|\boldsymbol{\varphi}^h\| = X$ for some finite value $X \in \mathbb{R}$.

Since both negative and positive electrodes satisfies the equations with the same structure, the linearization is derived for one electrode. For simplicity, the solid concentration is denoted by c_{k+1} for $k = 1, 2$ and the solid potential is indicated by φ_2. Let $\Delta\varphi^e = \varphi_2^e - \varphi_1^e$ and $\Delta\varphi^p = \varphi_2^p - \varphi_1^p$. From the boundary condition of solid concentration given by equations 2.19 and **??**,

$$\Delta\varphi = U_k(y_k) + \nu \sinh^{-1}(\iota_k(c_1, c_{k+1}) \frac{\partial c_{k+1}}{\partial r_k} \mid_{r_k = R_k}) \tag{3.14}$$

for $k = 1, 2$ where $\nu = 1/(\alpha_a F)$ and $\iota_k(c_1, c_{k+1}) = \frac{FD_{s,k}}{2i_{0,k}}(c_1, c_{k+1})$. After substituting the perturbation forms for the vectors $\boldsymbol{\varphi}$ and $\boldsymbol{c}$, given the formula in 2.13 for OCP term, and using equations 3.7, Taylor series expansion can be used on RHS of 3.14 to find

$$\Delta\varphi^p = t(\acute{U_k} \mid_{c_{k+1}^e} c_{k+1}^h \mid_{r_k = R_k} + \nu\iota_k \mid_{c_1^e, c_{k+1}^e} \frac{\partial c_{k+1}^h}{\partial r_k} \mid_{r_k = R_k} + O(t)) \tag{3.15}$$

where $|O(t)| \leq \delta t$ for some positive constant δ from Taylor's theorem. Since $\boldsymbol{c}^h \in \mathcal{C}$, the functions U_k, $\sinh^{-1}$, and ι_k are smooth, $\Delta\varphi^p = t\Delta\varphi^h = t(\varphi_2^h - \varphi_1^h)$ for some $\boldsymbol{\varphi}^h \in \mathcal{P}$.

Now, since equilibrium points are constant vectors and i_k is smooth at an equilibrium point where $\boldsymbol{c}^e$ is non-zero, by Taylor series expansion, the equation 2.8 takes the form

$$\frac{\partial}{\partial x}(\sigma^{eff} \frac{\varphi_2^p}{\partial x}) = t \sum a_k (\frac{\partial i_k}{\partial c_1} \mid_{c_1^e} c_1^h + \frac{\partial i_k}{\partial c_{k+1}} \mid_{c_{k+1}^e} c_{k+1}^h \mid r_k = R_k + \frac{\partial i_k}{\partial \Delta\varphi} \mid_{\Delta\varphi^e} \Delta\varphi^h + O(t)) \tag{3.16}$$

where $\Delta\varphi = \varphi_2 - \varphi_1$. The solution to equation 3.16 can be written as

$$\varphi_2^p = \frac{t}{\sigma^{eff}} \int_0^x \int_0^y \sum a_k (\frac{\partial i_k}{\partial c_1} \mid_{c_1^e} c_1^h + \frac{\partial i_k}{\partial c_{k+1}} \mid_{c_{k+1}^e} c_{k+1}^h \mid r_k = R_k + \frac{\partial i_k}{\partial \Delta\varphi} \mid_{\Delta\varphi^e} \Delta\varphi^h + O(t)) ds dy. \tag{3.17}$$

Taking absolute value from both sides of equation 3.17 results in

$$|\varphi_2^p| \leq \frac{tL^2}{\sigma^{eff}} \sum |a_k| (|\frac{\partial i_k}{\partial c_1} \mid_{c_1^e} \|c_1^h\| + |\frac{\partial i_k}{\partial c_{k+1}} \mid_{c_{k+1}^e} \|c_{k+1}^h\| + |\frac{\partial i_k}{\partial \Delta\varphi} \mid_{\Delta\varphi^e} \|\Delta\varphi^h\| + |O(t)|), \tag{3.18}$$

Therefor, $\varphi_2^p = t\varphi_2^h$ and $\varphi_2^p = t\varphi_2^h$ for some $\boldsymbol{\varphi}^h \in \mathcal{P}$. In the rest of linearization process, the perturbation form $\boldsymbol{\varphi} = \boldsymbol{\varphi}^e + t\boldsymbol{\varphi}^h$ is used.

The first nonlinear terms are i_k for $k = 1, 2$ composed of two nonlinear terms, $i_{0,k}$ and $\sinh(F(\varphi_2 - \varphi_1 - U_k(y_k))/(2RT))$. By Taylor series expansion, this term can be written as

$$i_k = i_{n,k}^e + t(I_{1,k}\varphi_2^h + I_{2,k}\varphi_1^h + I_{3,k}c_{k+1}^h \mid_{r_k=R_k} + I_{4,k}c_1^h) + o(t^2) \tag{3.19}$$

In a similar way other nonlinear terms take the form

$$\frac{1}{c_1^e + tc_1^h}\frac{\partial(c_1^e + tc_1^h)}{\partial x} = t\frac{1}{c_1^e}\frac{\partial c_1^h}{\partial x} + O(t^2) \tag{3.20}$$

$$k_D^{eff} \mid_{c_1^e + tc_1^h} = k_D^{eff} \mid_{c_1^e} + t\acute{k}_D^{eff} \mid_{c_1^e} c_1^h + O(t^2) \tag{3.21}$$

$$k^{eff} \mid_{c_1^e + tc_1^h} = k^{eff} \mid_{c_1^e} + t\acute{k}^{eff} \mid_{c_1^e} c_1^h + O(t^2) \tag{3.22}$$

$$D_{s,k} \mid_{c_{k+1}^e + tc_{k+1}^h} = D_{s,k} \mid_{c_{k+1}^e} + tD_{s,k}^{'} \mid_{c_{k+1}^e} c_{k+1}^h + O(t^2),\ k = 1, 2 \tag{3.23}$$

where $\acute{f}$ represents the differentiation with respect to the argument of f. The linearization parameters are given in table 3.1. In order to defined the state space representation of the linearized system, the new functions are defined

$$J_{k,r}(x) = \begin{cases} I_{k,r}(c_1^e, c_{k+1,n}^e, \varphi_1^e, \varphi_{2,n}^e) & \text{if } x \in [0, L_1] \\ 0 & \text{if } x \in [L_1, L_2] \\ I_{k,r}(c_1^e, c_{k+1,p}^e, \varphi_1^e, \varphi_{2,p}^e) & \text{if } x \in [0, L_1] \end{cases} \tag{3.24}$$

for $k = 1, 2$ and $r = 1 \cdots 4$.

Table 3.1: Linearization parameters

$i_{0,k}^e$	$(c_1^e)^{\alpha_a}\left(c_{s,max} - c_{k+1}^e\right)^{\alpha_a}\left(c_{k+1}^e\right)^{\alpha_c}$	$s_{3,k}$	$-\acute{U_k} \mid_{c_{k+1}^e} s_{1,k}$
$i_{1,k}$	$\alpha_a (c_1^e)^{\alpha_a - 1}\left(c_{s,max} - c_{k+1}^e\right)^{\alpha_a}(c_{k+1})^{\alpha_c}$	$i_{n,k}^e$	0
$i_{2,k}$	$\alpha_c (c_1^e)^{\alpha_a}\left(c_{s,max} - c_{k+1}^e\right)^{\alpha_a}\left(c_{k+1}^e\right)^{\alpha_c - 1}$	$I_{1,k}(c_1^e, c_{k+1}^e, \varphi_1^e, \varphi_2^e)$	$\frac{1}{2} i_{0,k}^e s_{1,k}$
	$-\alpha_a (c_1^e)^{\alpha_a}\left(c_{s,max} - c_{k+1}^e\right)^{\alpha_a - 1}\left(c_{k+1}^e\right)^{\alpha_c}$		
η_k^e	$\varphi_2^e - \varphi_1^e - U_k \mid_{c_{k+1}^e}$	$I_{2,k}(c_1^e, c_{k+1}^e, \varphi_1^e, \varphi_2^e)$	$\frac{1}{2} i_{0,k}^e s_{2,k}$
S_k^e	$sinh(\frac{F}{2RT}\eta_k^e)$	$I_{3,k}(c_1^e, c_{k+1}^e, \varphi_1^e, \varphi_2^e)$	$\frac{1}{2}(i_{0,j}^e s_{3,k} + S_k^e i_{2,k})$
$s_{1,k}$	$\frac{F}{2RT} cosh(\frac{F}{2RT}\eta_k^e)$	$I_{4,k}(c_1^e, c_{k+1}^e, \varphi_1^e, \varphi_2^e)$	$\frac{1}{2} S_k^e i_{1,k}$
$s_{2,k}$	$-s_{1,k}$		

Now, by substituting the perturbed variables and the results of equations 3.19-3.23 into state space representation equation 2.16 both RHS and LHS of the resulting equations can be divided by t; then, by letting $t \longrightarrow 0$, the linearized system is defined

by

$$\begin{bmatrix} \dot{\boldsymbol{c}} \\ 0 \end{bmatrix} = A^L \begin{bmatrix} \boldsymbol{c} \\ \boldsymbol{\varphi} \end{bmatrix} = \begin{bmatrix} A^L_{11} & A^L_{12} \\ A^L_{21} & A^L_{22} \end{bmatrix} \begin{bmatrix} \boldsymbol{c} \\ \boldsymbol{\varphi} \end{bmatrix} \tag{3.25}$$

where $A^L_{11} : \mathcal{C} \to \mathcal{X}$, $A^L_{12} : \mathcal{P} \to \mathcal{X}$, $A^L_{21} : \mathcal{C} \to \mathcal{Y}$, and $A^L_{22} : \mathcal{P} \to \mathcal{Y}$ are operator defined by

$$A^L_{11}\boldsymbol{c} = \begin{bmatrix} \frac{\partial}{\partial x}(D_e^{eff}\frac{\partial}{\partial x}c_1) + \frac{1-t^0}{F}\sum a_k J_{4,k}c_1 + \sum_{k=1,2}\sum_{j=n,s}(\frac{1-t^0}{F}a_k J_{3,k}c_{k+1,j} \mid_{r_k=R_k}) \\ \frac{1}{r_1^2}\frac{\partial}{\partial r_1}(D_{s,1} \mid_{c^e_{2,n}} r_1^2\frac{\partial}{\partial r_1}c_{2,n}) \\ \frac{1}{r_2^2}\frac{\partial}{\partial r_2}(D_{s,2} \mid_{c^e_{3,n}} r_2^2\frac{\partial}{\partial r_2}c_{3,n}) \\ \frac{1}{r_1^2}\frac{\partial}{\partial r_1}(D_{s,1} \mid_{c^e_{2,p}} r_1^2\frac{\partial}{\partial r_2}c_{2,p}) \\ \frac{1}{r_2^2}\frac{\partial}{\partial r_2}(D_{s,2} \mid_{c^e_{3,p}} r_2^2\frac{\partial}{\partial r_2}c_{3,p}) \end{bmatrix}$$

$$A^L_{12}\boldsymbol{\varphi} = \begin{bmatrix} \frac{1-t^0}{F}\sum a_k J_{2,k}\varphi_1 + \sum_{j=n,p}(\frac{1-t^0}{F}\sum a_k J_{1,k}\varphi_{2,j}) \\ 0 \end{bmatrix}$$

$$A^L_{21}\boldsymbol{c} = \begin{bmatrix} \frac{\partial}{\partial x}(\frac{1}{c_1^e}k^{eff} \mid_{c_1^e} \frac{\partial}{\partial x}c_1) - \sum a_k J_{4,k}c_1 - \sum_{k=1,2}\sum_{j=n,s}(a_k J_{3,k}c_{k+1,j} \mid_{r_k=R_k}) \\ -\sum a_k J_{4,k}c_1 - \sum_{k=1,2}\sum_{j=n,s}(a_k J_{3,k}c_{k+1,j} \mid_{r_k=R_k}) \\ -\sum a_k J_{4,k}c_1 - \sum_{k=1,2}\sum_{j=n,s}(a_k J_{3,k}c_{k+1,j} \mid_{r_k=R_k}) \end{bmatrix}$$

$$A^L_{22}\boldsymbol{\varphi} = \begin{bmatrix} \frac{\partial}{\partial x}(-k^{eff} \mid_{c_1^e} \frac{\partial}{\partial x}\varphi_1) - \sum a_k J_{2,k}\varphi_1 - \sum_{j=n,p}(\sum a_k J_{1,k}\varphi_{2,j}) \\ -\sum a_k J_{2,k}\varphi_1 + \frac{\partial}{\partial x}(\sigma^{eff}\frac{\partial}{\partial x}\varphi_{2,n}) - \sum a_k J_{1,k}\varphi_{2,n} \\ -\sum a_k J_{2,k}\varphi_1 + \frac{\partial}{\partial x}(\sigma^{eff}\frac{\partial}{\partial x}\varphi_{2,p}) - \sum a_k J_{1,k}\varphi_{2,p} \end{bmatrix}$$

Similarly, the linearized boundary conditions are obtained by ignoring the effect of terms of order t^2 as

$$\frac{\partial \varphi_1}{\partial x} \mid_{x=0} = \frac{\partial \varphi_1}{\partial x} \mid_{x=L} = 0 \tag{3.26}$$

$$\varphi_{2,n} \mid_{x=0} = 0 \tag{3.27}$$

$$\frac{\partial \varphi_{2,n}}{\partial x} \mid_{x=L_1} = 0 \tag{3.28}$$

$$\frac{\partial \varphi_{2,p}}{\partial x} \mid_{x=L_2} = 0 \tag{3.29}$$

$$\frac{\partial c_1}{\partial x} \mid_{x=0} = \frac{\partial c_1}{\partial x} \mid_{x=L} = 0 \tag{3.30}$$

$$\frac{\partial c_{k+1,n}}{\partial r_k} \mid_{r_k=0} = 0 \tag{3.31}$$

$$\frac{\partial c_{k+1,n}}{\partial r_k} \mid_{r_k=R_k} = \frac{J_{1,k}\varphi_{2,n} + J_{2,k}\varphi_1 + \sum_{r=1,2} J_{3,r} c_{r+1,n} \mid_{r_r=R_r} + J_{4,k} c_1}{D_{s,k} \mid c^e_{k+1,n} F}, \quad k = 1, 2 \tag{3.32}$$

$$\frac{\partial c_{k+1,p}}{\partial r_k} \mid_{r_k=0} = 0 \tag{3.33}$$

$$\frac{\partial c_{k+1,p}}{\partial r_k} \mid_{r_k=R_k} = \frac{J_{1,k}\varphi_{2,p} + J_{2,k}\varphi_1 + \sum_{r=1,2} J_{3,r} c_{r+1,p} \mid_{r_r=R_r} + J_{4,k} c_1}{D_{s,k} \mid c^e_{k+1,p} F}, \quad k = 1, 2 \tag{3.34}$$

The boundary control is

$$\sigma^{eff} \frac{\partial \varphi_{2,p}}{\partial x} \mid_{x=L} = I(t) \tag{3.35}$$

Chapter 4

Research plan

The aim of this project is to accurately predict the SOC of a Li-ion battery in HEV real time application. The suggested methods in literature are categorized in three groups, direct measurement, book-keeping method, and model based estimation. Among them, the model based estimation is granted for real time SOC estimation in the HEVs due to their accuracy. As an important part of model based estimation, the cell mathematical equation must be evaluated. Because of being accurate and physical, the electrochemical modeling is used in this research.

In the process of improving a simplified model, the main characteristics of the original governing equation must be preserved. These characteristics includes equilibrium points determined in chapter 3 and their properties. Multiplicity and different stability properties of the equilibrium points results in an important characteristic of the governing equations called hysteresis. Therefor, the model used for estimation design should posses the same equlibria. OCP also is a source of hysteresis, and its effect on the system behavior must be transferred to the simplified model.

4.1 Modeling improvement and simplification

Linear approximation is a simplified model presented in chapter 3. In this approximation, the original governing equations are linearized around their equilibria; However, there are more than one equilibria. There are two ways of dealing with this problem. As the first option, the equilibrium point at initial condition can be picked. A more efficient way is to employ more than one equilibrium points depending on the path enforced by the input current to the system.

For every electrode, given a prediction of left amount of active material $\Delta c_{k+1,j}$, the equilibrium solution for solid concentration is attained by $\Delta c_{k+1,j}/(\epsilon_{s,k} v_e)$ where v is the volume of electrode. Subindices k and j correspond respectively to the electrode and size bin of interest; $j = n$ for negative electrode, $j = p$ for positive electrode, and $k = 1, 2$. The left amount of active material can be predicted by conservation law stated as

$$\dot{c}^e_{k+1,j} = s\frac{I(t)}{F v_e(\epsilon_{s,1} + \epsilon_{s,2})},\ c^e_{k+1,j}\ |_{t=0} = c^0_{k+1,j}. \tag{4.1}$$

Moreover, according to the equations 3.7 and 3.13, the elements of equilibrium solution of the system 2.16 are shown to be functions of equilibrium solid concentration. Now, the system can be linearized around a path rather than a point.

The linearized equations around the path given by equation 4.1 include the same equations as in equation 2.16 except for control term. The state space representation takes the form

$$\begin{bmatrix} \dot{\boldsymbol{c}} \\ 0 \end{bmatrix} = A^L \begin{bmatrix} \boldsymbol{c} \\ \boldsymbol{\varphi} \end{bmatrix} + \begin{bmatrix} 0 \\ -\frac{1}{v_e \epsilon_{s,1} F} \\ -\frac{1}{v_e \epsilon_{s,2} F} \end{bmatrix} I(t) \tag{4.2}$$

Therefore, the linearized equation 4.2 augmented with boundary condition 3.26-3.35 and the ODE 4.1 construct a simplified system of equations and will be used for design of estimation method.

In the process of finding the equilibrium points, the OCP term was set to be a single input-single output mapping. The validity of this assumption depends on the sensitivity of the system states to the OCP hysteretic behavior. Substituting the OCP term by a hysteresis operator can both change the location of equilibria and the stability properties around every specific equilibrium point. In addition, OCP often exhibits a rate dependent hysteresis in Li-ion batteries. The effect of OCP on the system states can either be observed through simulation or analyzing the equilibrium points. In order to improve the model, these question must be answered: Is hysteresis required to be included in the OCP term? Which hysteresis operator should be used to model OCP term?

Typically, simplified governing equations also form a system of PDAEs; nevertheless, most of the observer design are specified to systems of PDEs. In this case, the constraint equations needs to be solved for the vector $\boldsymbol{\varphi}$ such that they can be eliminated. In contrast to original governing equations, in the case of linearized system, constraint equations admit an approximate explicit solution. In order to attain this approximate

solution the state space representation of constraint equations given by 3.25 is written as

$$A_{12}^{L}\boldsymbol{\varphi} = -A_{11}^{L}\boldsymbol{c}. \tag{4.3}$$

Given boundary conditions 3.26-3.28 and the RHS of equation 4.3 as the source term, Galerkin method can be used to approximate the solution. In this approach, $\boldsymbol{\varphi}$ is written in terms of the eigenfunctions of the operator A_{12}. Substituting the result into 3.25 converts PDAEs to a set of PDEs.

4.2 Model based observer design

After improving a simplified model for real time application, a proper observation method needs to be defined. Observability condition of the state vector is the first must-be-checked step in forming a model based estimation. Two important versions of observability condition are typically introduced in control utilization: strong and approximate observability. Because of being easier to check, approximate observability is preferred. However, this condition can hardly be investigated for nonlinear systems especially for distributed parameter systems. In this research, the linear approximation is used to test the observability condition and the result is extended to the original equations.

For every electrode, the state of charge can be defined as a function of solid concentrations by

$$SOC = \frac{\theta_b - \theta_0}{\theta_{100} - \theta_0} \tag{4.4}$$

where

$$\theta_b = \frac{3\sum_k \epsilon_s \int_0^{R_k} r_k^2 c_{k+1}(r_k, x, t) dr_k}{c_{s,max}\sum_k \epsilon_s R_k^3} \tag{4.5}$$

where $c_{k+1} = c_{k+1,n}$ for negative and $c_{k+1} = c_{k+1,p}$ for positive electrode. Therefore, approximate observability of solid concentrations, the last K elements of the state vector assigned to K groups of particles, is expected.

In the next step, the resultant PDEs is often approximated by ODEs depending before proceeding to observer design. In this case, the governing equations are approximated by nth order ODEs which limit goes to the original equations. Discretizing in space via finite element method (FEM) is the suggested to construct the ODEs. The dimension of the resultant system of ODEs can be chosen large to increase accuracy; then, this large system can be truncated without loosing much accuracy. Two important methods are introduced in [2] to reduce the dimension of the system of ODEs, balanced truncation

method and proper orthogonal decomposition method. The truncation can be both applied before or after observer design respectively to system model and observer model.

Above all, an observer must be adapted to add robustness to the truncated dynamics and modeling uncertainties. Since a common observer is composed of a copy of system model and a feedback term, the robustness can be provided by a proper choice of feedback term. Adding more simplification and order reduction to the original equation necessitates a more robust feedback design. In the absence of uncertainties, Luenberger observer is frequently used in which the output estimation error, the difference between the system measured output and the observer calculated output, is linearly fed back into the observer. However, it loses error convergence to zero [50].

Sliding mode observer (SMO) provides an alternative solution to handle modeling truncation and uncertainties. In this observer, the output estimation error is fed back to the observer via a nonlinear switching term. Asymptotic convergence of estimation error in a finite time is achievable by SMO when a bound is provided on the norm of modeling truncation and uncertainties [50]. On unique properties of SMO , the sliding motion of the estimation error ensuring that the state estimates are precisely comparable with the actual sate of the system can be addressed. This unique property and the robustness provided by SMO have made it a promising method in recent years.

SMO is suggested here in which the linearized system around the path of equilibrium points presented in equations 4.1 and 4.2 are employed in the observer design. Although the problem of designing the SMO is well studied for lumped parameter systems, there are less research on its extension to distributed parameter systems. For this reason, PDEs are first transformed to a set of ODEs as described before; then, the observer is constructed for obtained ODEs. In order to complete the design process, the validity of the approximated observer must be checked. In this case, some critical questions must be answered: Is the assumption of boundedness of modeling uncertainties valid? Are the observers constructed for ODEs with different dimension converges to an observer for the original system?

At this point the SMO is introduced briefly. Let the system have the following representation,

$$\begin{aligned} \dot{\boldsymbol{z}} &= A_L \boldsymbol{z} + A_N \boldsymbol{z} + B\boldsymbol{u} \\ y &= h(\boldsymbol{z}) \end{aligned} \tag{4.6}$$

where $\boldsymbol{z} \in \mathbb{R}^n$ is the state vector, $\boldsymbol{u} \in \mathbb{R}^m$ is the control vector, $y \in \mathbb{R}$ is the output vector, A_L is the linearized operator around the path of equilibria, A_N is the uncertainty term, B is a linear control operator, and h is a nonlinear output function. From generalizing

the idea of sliding mode observer for ODEs in [58, 9, 10], the vector function $H(\boldsymbol{z}) = [h_1(\boldsymbol{z}), \cdots, h_n(\boldsymbol{z})]$ is introduced wherein

$$h_1(\boldsymbol{z}) = h(\boldsymbol{z})$$
$$h_i(\boldsymbol{z}) = \frac{\partial h_{i-1}(\boldsymbol{z})}{\partial \boldsymbol{z}} A_L \boldsymbol{z}, \quad i = 2 \cdots n$$

Next, the observer is defined by

$$\dot{\hat{\boldsymbol{z}}} = A_L \hat{\boldsymbol{z}} + B\boldsymbol{u} + (\frac{\partial H}{\partial \boldsymbol{z}})^{-1} \mid_{\boldsymbol{z}=\hat{\boldsymbol{z}}} N(y - h(\hat{\boldsymbol{z}})) + (\frac{\partial H}{\partial \boldsymbol{z}})^{-1} \mid_{\boldsymbol{z}=\hat{\boldsymbol{z}}} M(\hat{\boldsymbol{z}}) sign(W(t)) \tag{4.7}$$

where $M(\hat{\boldsymbol{z}}) = diag\,[m_1(\hat{\boldsymbol{z}}), \cdots, m_n(\hat{\boldsymbol{z}})]$ is a diagonal matrix, $W(t) = [w_1(t), \cdots, w_n(t)]^T$ and

$$w_1(t) = y - h(\hat{\boldsymbol{z}})$$
$$w_{i+1}(t) = \{m_i(\hat{\boldsymbol{z}}) sign(w_i(t))\}_{eq}, \quad i = 1 \cdots n-1$$

where $\{\}_{eq}$ stands for an equivalent value operator of a discontinuous function in sliding mode.

Given the finite dimensional representation of the system, Lyapunov theory will be used to calculate the gains, N and $M(\hat{\boldsymbol{z}})$, and the imposed conditions such that the estimation error become asymptotically stable around zero. This conditions depend on the structure and properties of the nonlinear term $A_N \boldsymbol{z}$ which is truncated in observer dynamics. Boundedness is one of these properties and must be investigated first. Furthermore, the observers designed for the approximate finite dimensional systems must converge to an observer for the original system. In this case, both validity of projecting the nonlinear term onto a finite dimensional space and convergence properties of the operator used for sliding mode feedback need to be checked.

In a similar way, Lyapunov method can be applied in a distributed parameter system for stability proof; however, more condition must be check while using the Lyapunov theory in infinite dimensional space. Most of the time these conditions including compactness of initiated trajectories by PDEs are not easy to checked. More easier and logical methodology of dealing with the problem of tuning the gains is to project the operating space onto finite dimensional approximate spaces. This approach is concerned in this research due to its physical interpretation and simplicity.

After all, the improved observer should be extended to be applicable in more general applications. The effects of temperature and battery aging on electrochemical parameters of the governing equations are important issues and should be included in SOC

estimation. This can be done by extending the governing equation or enhancing the observer with an adaptive scheme. Finally, SOC estimation should be generalized to be applicable for a battery stack whose components are the studied cells. This generalization is attained by simply finding the current distribution over the battery cells.

4.3 Time table

	Spring 2014	**Fall 2014**	**Winter 2015**	**Spring 2015**
Stability analysis of equilibria				
Investigating the effect of OCP hysteresis and its modeling				
Approximating the constraint equations				
Observability check of the linearized system				
Finite dimensional approximation of PDEs				
Checking the boundedness of nonlinear terms				
Sliding mode observer design for approximated finite dimensional system of a cell				
Checking the convergence of finite dimensional observers				
Generalizing the observer to include the electro-chemical parameters variation				
Extending the observer to SOC estimation of the battery stack				

	Fall 2015	**Winter 2016**	**Spring 2016**
Refining model and experiment			
Thesis preparation			

Bibliography

[1] J. Alzieu, H. Smimite, and C. Glaize. Improvement of intelligent battery controller: state-of-charge indicator and associated functions. *Journal of power sources*, 67(1):157–161, 1997.

[2] A. C. Antoulas. *Approximation of large-scale dynamical systems*, volume 6. Siam, 2005.

[3] B. Bhangu, P. Bentley, D. Stone, and C. Bingham. Observer techniques for estimating the state-of-charge and state-of-health of vrlabs for hybrid electric vehicles. In *Vehicle Power and Propulsion, 2005 IEEE Conference*, pages 10–pp. IEEE, 2005.

[4] O. Caumont, P. Le Moigne, C. Rombaut, X. Muneret, and P. Lenain. Energy gauge for lead-acid batteries in electric vehicles. *Energy Conversion, IEEE Transactions on*, 15(3):354–360, 2000.

[5] F. Codecà, S. M. Savaresi, and G. Rizzoni. On battery state of charge estimation: A new mixed algorithm. In *Control Applications, 2008. CCA 2008. IEEE International Conference on*, pages 102–107. IEEE, 2008.

[6] D. Di Domenico, A. Stefanopoulou, and G. Fiengo. Lithium-ion battery state of charge and critical surface charge estimation using an electrochemical model-based extended kalman filter. *Journal of Dynamic Systems, Measurement, and Control*, 132(6):061302, 2010.

[7] D. V. Do, C. Forgez, K. El Kadri Benkara, and G. Friedrich. Impedance observer for a li-ion battery using kalman filter. *Vehicular Technology, IEEE Transactions on*, 58(8):3930–3937, 2009.

[8] M. Doyle, T. F. Fuller, and J. Newman. Modeling of galvanostatic charge and discharge of the lithium/polymer/insertion cell. *Journal of the Electrochemical Society*, 140(6):1526–1533, 1993.

[9] S. Drakunov and V. Utkin. Sliding mode observers. tutorial. In *Decision and Control, 1995., Proceedings of the 34th IEEE Conference on*, volume 4, pages 3376–3378. IEEE, 1995.

[10] S. V. Drakunov and M. Reyhanoglu. Hierarchical sliding mode observers for distributed parameter systems. *Journal of Vibration and Control*, 17(10):1441–1453, 2011.

[11] M. Farkhondeh and C. Delacourt. Mathematical modeling of commercial lifepo4 electrodes based on variable solid-state diffusivity. *Journal of The Electrochemical Society*, 159(2):A177–A192, 2011.

[12] M. Farkhondeh, M. Safari, M. Pritzker, M. Fowler, T. Han, J. Wang, and C. Delacourt. Full-range simulation of a commercial lifepo4 electrode accounting for bulk and surface effects: A comparative analysis. *Journal of The Electrochemical Society*, 161(3):A201–A212, 2014.

[13] M. Giaquinta and G. Modica. *Mathematical analysis: an introduction to functions of several variables*. Springer, 2010.

[14] H. He, R. Xiong, and J. Fan. Evaluation of lithium-ion battery equivalent circuit models for state of charge estimation by an experimental approach. *energies*, 4(4):582–598, 2011.

[15] X. Hu, S. Li, and H. Peng. A comparative study of equivalent circuit models for li-ion batteries. *Journal of Power Sources*, 198:359–367, 2012.

[16] Y. Hu and S. Yurkovich. Battery state of charge estimation in automotive applications using lpv techniques. In *American Control Conference (ACC), 2010*, pages 5043–5049. IEEE, 2010.

[17] F. Huet. A review of impedance measurements for determination of the state-of-charge or state-of-health of secondary batteries. *Journal of power sources*, 70(1):59–69, 1998.

[18] B. Jun, S. Sai, G. Wei, and W. Lu. State of charge estimation of li-ion batteries in an electric vehicle based on a radial-basis-function neural network. *Chinese Physics B*, 21(11):118801, 2012.

[19] I.-S. Kim. The novel state of charge estimation method for lithium battery using sliding mode observer. *Journal of Power Sources*, 163(1):584–590, 2006.

[20] I.-S. Kim. Nonlinear state of charge estimator for hybrid electric vehicle battery. *Power Electronics, IEEE Transactions on*, 23(4):2027–2034, 2008.

[21] R. Klein, N. A. Chaturvedi, J. Christensen, J. Ahmed, R. Findeisen, and A. Kojic. State estimation of a reduced electrochemical model of a lithium-ion battery. In *American Control Conference (ACC), 2010*, pages 6618–6623. IEEE, 2010.

[22] R. Klein, N. A. Chaturvedi, J. Christensen, J. Ahmed, R. Findeisen, and A. Kojic. Electrochemical model based observer design for a lithium-ion battery. 2012.

[23] K. Kutluay, Y. Cadirci, Y. S. Ozkazanc, and I. Cadirci. A new online state-of-charge estimation and monitoring system for sealed lead-acid batteries in telecommunication power supplies. *Industrial Electronics, IEEE Transactions on*, 52(5):1315–1327, 2005.

[24] D.-T. Lee, S.-J. Shiah, C.-M. Lee, and Y.-C. Wang. State-of-charge estimation for electric scooters by using learning mechanisms. *Vehicular Technology, IEEE Transactions on*, 56(2):544–556, 2007.

[25] M.-F. Li, W. Chen, H. Wu, and D. Gorski. Robust state of charge estimation of lithium-ion batteries via an iterative learning observer. *Training*, 2011:11–04, 2012.

[26] Y. Li, R. D. Anderson, J. Song, A. M. Phillips, and X. Wang. A nonlinear adaptive observer approach for state of charge estimation of lithium-ion batteries. In *American Control Conference (ACC), 2011*, pages 370–375. IEEE, 2011.

[27] M. Mastali, J. Vazquez-Arenas, R. Fraser, M. Fowler, S. Afshar, and M. Stevens. Battery state of the charge estimation using kalman filtering. *Journal of Power Sources*, 239:294–307, 2013.

[28] K. Morris. What is hysteresis? *Applied Mechanics Reviews*, 64(5):050801, 2011.

[29] S. Moura, N. Chaturvedi, and M. Krstic. Pde estimation techniques for advanced battery management systemspart i: Soc estimation. In *American Control Conference (ACC), 2012*, pages 559–565. IEEE, 2012.

[30] S. J. Moura, N. A. Chaturvedi, and M. Krstić. Adaptive partial differential equation observer for battery state-of-charge/state-of-health estimation via an electrochemical model. *Journal of Dynamic Systems, Measurement, and Control*, 136(1):011015, 2014.

[31] S. J. Moura, M. Krstic, and N. A. Chaturvedi. Adaptive pde observer for battery soc/soh estimation. In *ASME 2012 5th Annual Dynamic Systems and Control Conference joint with the JSME 2012 11th Motion and Vibration Conference*, pages 101–110. American Society of Mechanical Engineers, 2012.

[32] N. K. MSirdi, A. Belhani, and A. Naamane. Battery models for estimation of state of charge by sliding mode observer. In *Sustainability in Energy and Buildings*, pages 133–149. Springer, 2012.

[33] S. Pang, J. Farrell, J. Du, and M. Barth. Battery state-of-charge estimation. In *American Control Conference, 2001. Proceedings of the 2001*, volume 2, pages 1644–1649. IEEE, 2001.

[34] S. Piller, M. Perrin, and A. Jossen. Methods for state-of-charge determination and their applications. *Journal of power sources*, 96(1):113–120, 2001.

[35] G. L. Plett. Extended kalman filtering for battery management systems of lipb-based hev battery packs: Part 1. background. *Journal of Power sources*, 134(2):252–261, 2004.

[36] G. L. Plett. Extended kalman filtering for battery management systems of lipb-based hev battery packs: Part 2. modeling and identification. *Journal of power sources*, 134(2):262–276, 2004.

[37] G. L. Plett. Extended kalman filtering for battery management systems of lipb-based hev battery packs: Part 3. state and parameter estimation. *Journal of Power sources*, 134(2):277–292, 2004.

[38] G. L. Plett. Sigma-point kalman filtering for battery management systems of lipb-based hev battery packs: Part 2: Simultaneous state and parameter estimation. *Journal of Power Sources*, 161(2):1369–1384, 2006.

[39] V. Pop, H. Bergveld, and P. Regtien. Smart and accurate state-of-charge indication in portable applications. In *Power Electronics and Drives Systems, 2005. PEDS 2005. International Conference on*, volume 1, pages 262–267. IEEE, 2005.

[40] V. Pop, H. J. Bergveld, J. O. het Veld, P. Regtien, D. Danilov, and P. Notten. Modeling battery behavior for accurate state-of-charge indication. *Journal of the Electrochemical Society*, 153(11):A2013–A2022, 2006.

[41] V. Prajapati, H. Hess, E. William, V. Gupta, M. Huff, M. Manic, F. Rufus, A. Thakker, and J. Govar. A literature review of state of-charge estimation techniques applicable to lithium poly-carbon monoflouride (li/cfx) battery. In *Power Electronics (IICPE), 2010 India International Conference on*, pages 1–8. IEEE, 2011.

[42] A. H. Ranjbar, A. Banaei, A. Khoobroo, and B. Fahimi. Online estimation of state of charge in li-ion batteries using impulse response concept. *Smart Grid, IEEE Transactions on*, 3(1):360–367, 2012.

[43] S. Rodrigues, N. Munichandraiah, and A. Shukla. A review of state-of-charge indication of batteries by means of ac impedance measurements. *Journal of Power Sources*, 87(1):12–20, 2000.

[44] P. Rong and M. Pedram. An analytical model for predicting the remaining battery capacity of lithium-ion batteries. *Very Large Scale Integration (VLSI) Systems, IEEE Transactions on*, 14(5):441–451, 2006.

[45] M. A. Roscher and D. U. Sauer. Dynamic electric behavior and open-circuit-voltage modeling of lifepo¡ sub¿ 4¡/sub¿-based lithium ion secondary batteries. *Journal of Power Sources*, 196(1):331–336, 2011.

[46] A. J. Salkind, C. Fennie, P. Singh, T. Atwater, and D. E. Reisner. Determination of state-of-charge and state-of-health of batteries by fuzzy logic methodology. *Journal of Power Sources*, 80(1):293–300, 1999.

[47] S. Santhanagopalan, Q. Guo, P. Ramadass, and R. E. White. Review of models for predicting the cycling performance of lithium ion batteries. *Journal of Power Sources*, 156(2):620–628, 2006.

[48] S. Santhanagopalan and R. E. White. Online estimation of the state of charge of a lithium ion cell. *Journal of Power Sources*, 161(2):1346–1355, 2006.

[49] S. Santhanagopalan and R. E. White. State of charge estimation using an unscented filter for high power lithium ion cells. *International Journal of Energy Research*, 34(2):152–163, 2010.

[50] Y. Shtessel, C. Edwards, L. Fridman, and A. Levant. *Sliding mode control and observation*. Springer, 2014.

[51] K. A. Smith, C. D. Rahn, and C.-Y. Wang. Model-based electrochemical estimation of lithium-ion batteries. In *Control Applications, 2008. CCA 2008. IEEE International Conference on*, pages 714–719. IEEE, 2008.

[52] K. A. Smith, C. D. Rahn, and C.-Y. Wang. Model-based electrochemical estimation and constraint management for pulse operation of lithium ion batteries. *Control Systems Technology, IEEE Transactions on*, 18(3):654–663, 2010.

[53] V. Srinivasan and J. Newman. Discharge model for the lithium iron-phosphate electrode. *Journal of the Electrochemical Society*, 151(10):A1517–A1529, 2004.

[54] K. Thomas, J. Newman, and R. Darling. Mathematical modeling of lithium batteries. *Advances in lithium-ion batteries*, pages 345–392, 2002.

[55] I. V. Thorat. *Understanding Performance-limiting Mechanisms in Lithium-ion Batteries for High-rate Applications*. ProQuest, 2009.

[56] W. van Schalkwijk and B. Scrosati. *Advances in lithium-ion batteries*. Springer, 2002.

[57] A. Vasebi, S. Bathaee, and M. Partovibakhsh. Predicting state of charge of lead-acid batteries for hybrid electric vehicles by extended kalman filter. *Energy Conversion and Management*, 49(1):75–82, 2008.

[58] K. Veluvolu, Y. Soh, and W. Cao. Robust observer with sliding mode estimation for nonlinear uncertain systems. *Control Theory & Applications, IET*, 1(5):1533–1540, 2007.

[59] M. Verbrugge. Adaptive, multi-parameter battery state estimator with optimized time-weighting factors. *Journal of Applied Electrochemistry*, 37(5):605–616, 2007.

[60] M. Verbrugge and E. Tate. Adaptive state of charge algorithm for nickel metal hydride batteries including hysteresis phenomena. *Journal of Power Sources*, 126(1):236–249, 2004.